Journal of Computational Physics 228 (2009) 2934–2950

Contents lists available at ScienceDirect

Journal of Computational Physics

journal homepage: www.elsevier.com/locate/jcp

# Conservative discretization of Coriolis force in a finite volume framework

E. Audusse [a,*], R. Klein [b], A. Owinoh [b]

[a] Université Paris 13, 99 Avenue, J.B. Clément, 93430 Villetaneuse, France
[b] Freie Universität Berlin, 2-6 Arnimallee, 14195 Berlin, Germany

ARTICLE INFO

*Article history:*
Received 19 November 2007
Received in revised form 5 January 2009
Accepted 6 January 2009
Available online 16 January 2009

*Keywords:*
Shallow water flows
Rotational fluids
Coriolis force
Conservation property
Linear momentum
Finite volume method

ABSTRACT

In this article we are interested in the problem of numerical simulations for a shallow fluid flow in a rotating system. This problem is closely related to climate or meteorological simulations. Our purpose is to introduce a new finite volume technique which allows us to guarantee conservation of linear momentum in an inertial frame of reference. Furthermore, we show that this method introduces a new discrete Coriolis term which is based on the interface mass fluxes instead of on straightforward cell-centered evaluation of the source term. Some numerical tests exhibit that this approach significantly reduces the numerical diffusion and is particularly interesting when considering nonisotropic meshes or long time simulations.



## 1. Introduction

In 1835 Coriolis [6] showed that a rotating frame can be considered as a reference frame if two forces, the Coriolis and centrifugal forces, are added. The centrifugal force affects all the particles of fluid and its direction is purely radial in the rotating system. The Coriolis force concerns only particles that undergo relative motion in the relative frame and it is orthogonal to their velocities, and to the axis of rotation. It follows that in a rotating frame the shallow water equations are classically written in the form of

$$\begin{cases} (\partial_t h)_r + \nabla_r \cdot (h\mathbf{u}) = 0, \\ (\partial_t (h\mathbf{u}))_r + \nabla_r \cdot (h\mathbf{u} \otimes \mathbf{u}) + \nabla_r \left(\frac{gh^2}{2}\right) + 2\boldsymbol{\Omega} \times (h\mathbf{u}) + h\boldsymbol{\Omega} \times (\boldsymbol{\Omega} \times \mathbf{x}^r) = 0, \end{cases} \tag{1}$$

where $h(t, \mathbf{x}^r)$ is the fluid height, $\mathbf{u}(t, \mathbf{x}^r)$ is the velocity, $\boldsymbol{\Omega}$ is the vector of rotation, $g$ is the acceleration due to the gravity, and the sub- or superscript $r$ is related to the fact that we consider all the coordinates and derivatives in the relative frame. The symbol $\times$ and $\otimes$ denote the vector and tensorial products, respectively. This result can easily be obtained by considering the equations in the inertial frame

* Corresponding author.
*E-mail address:* audusse@math.univ-paris13.fr (E. Audusse).

0021-9991/$ - see front matter © 2009 Elsevier Inc. All rights reserved.
doi:10.1016/j.jcp.2009.01.004

$$\begin{cases} (\partial_t \hat{h})_i + \nabla_i \cdot (\hat{h}\hat{\mathbf{u}}) = 0, \\ (\partial_t (\hat{h}\hat{\mathbf{u}}))_i + \nabla_i \cdot (\hat{h}\hat{\mathbf{u}} \otimes \hat{\mathbf{u}}) + \nabla_i \left(\frac{g\hat{h}^2}{2}\right) = 0 \end{cases} \tag{2}$$

and applying an appropriate coordinate transformation to the rotating frame. In system (2), $\hat{h}(t, \mathbf{x}^i)$ is the fluid height, $\hat{\mathbf{u}}(t, \mathbf{x}^i)$ is the velocity, and the sub- or superscript $i$ is related to the fact that we consider all the coordinates and derivatives in the inertial frame.

Now we are interested in the numerical discretization of systems (1) or (2). We are motivated by many important applications in meteorology and climate research [14,18,20]. System (1), written in the relative frame, has many advantages. It allows us to access immediately the quantities of interest (the wind velocity on the earth, for example, and not the wind velocity plus the velocity due to the rotation of the earth). Also the computational domain and, in many computer models, the related mesh are fixed. But it has also important drawbacks since we loose some information related to the inertial quantities. In particular let us observe that the inertial momentum has to be preserved since (2) is a homogeneous system in conservation form. This property remains obviously satisfied by the continuous relative system (1), but is now due to some balancing phenomenon between flux and source terms which is not easy to extend to the discrete level even if the discretization technique is conservative. This problem is well known in the context of shallow water equations with topographic source term, see [1,3] and references therein, or Euler equations with gravity terms, see [2]. This lack of conservativity of the classical discretizations is the main motivation for the present work. It stems from the fact that, in practical applications in meteorology or climate research, one can hardly ever completely resolve all flow features, so that nearly converged solutions are the exception rather than the rule. The integral conservation laws for mass, linear momentum, and total energy in gasdynamics or mass and linear momentum in the shallow water context are, however, valid on arbitrary control volumes without any convergence requirement – provided accurate approximations for the effective fluxes of the conserved quantities are available. A fully conservative scheme is therefore of interest in building computational models whose fundamental design principles remain valid even if the solutions are strongly underresolved. In a recently published article, Thurburn [18] presents a detailed review of the relative importance of different conservation properties and the need to preserve such properties in numerical weather prediction and climate models. The argument for such a need is strong for long-term climate simulations, as numerical sources and sinks can degrade the accuracy of the various global budgets significantly over a long time. Thuburn [18] also discusses how numerical models can ensure the desired conservation properties through discretization procedures. In this study we present a new discretization technique that guarantees conservation of linear inertial momentum. The heart of the method is to change the order of the processes that are involved in the transition from the continuous inertial equations to the discrete relative ones. The classical way is to perform the change of variables at the continuous level and then to discretize the relative system (1). Here we first apply a conservative discretization method to the inertial system (2) and then we perform the change of reference frame in order to exhibit a set of equations that involves the discrete relative fluid height and momentum. This method will have the inherent property of being conservative for the linear inertial momentum. Furthermore this new method preserves the advantages of the classical one since the effective computations are performed on the discrete relative quantities and on a fixed mesh.

In global climate or meteorological simulations the problem is posed on the sphere. In this case centrifugal forces are often included in the pressure and/or gravity term. Hence it is fundamental to be able to distinguish the Coriolis and centrifugal effects in our new discretization. It is done in the second part of this article. The discrete Coriolis effect is proved to be modelled through two distinguished terms. The first one involves the cell-centered momentum and is similar to the classical approximation. The second one involves the mass fluxes through the cell interfaces and thus can be interpreted as a discretization of the momentum flux due to rotation of the cell interfaces. These two terms are equal in the continuous limit and are the direct analogues of the well-known two terms that arise in the transformation to a rotating system on the level of the underlying partial differential equations (1). Numerical investigation exhibit that the resulting "crosswind scheme" is insensitive to anisotropy of the computational mesh, which is not the case for the classical centered discretization.

Throughout the paper we consider the shallow water equations on a rotating plane. This allows us to focus on the details of our new approach without having to deal with other technical difficulties. We do insist, though, on the fact that our approach is quite general and is absolutely applicable to a wide range of equations, including the 3D Euler equations on the sphere. The reason for our insisting is that the principal sequence of steps, namely

(1) discretize the conservation laws formulated in an inertial frame for a time dependent grid;
(2) transform the discrete equations into the grid-attached frame for both the space–time coordinates and the dependent variables;
(3) regroup the resulting equations so as to identify the terms corresponding to the Coriolis- and centrifugal accelerations makes no reference to either a specific set of conservation laws, and neither does it assume flat geometry of the flow domain.

The outline of the paper is as follows. In Section 2 we perform the discretization of the inertial equations on a rotating mesh, from which we can derive a conservative scheme. Then we go a step further and we identify the Coriolis and centrifugal forces in the new formulation. Then we prove that our scheme is consistent with the continuous equations. Finally we present some numerical tests that illustrate the capabilities of the method in Section 3.

## 2. A conservative scheme for rotating shallow flows

In this section we describe our new method to solve the problem of a shallow moving fluid on a rotational domain. The main goal is to ensure the conservation of the discrete inertial momentum. We first exhibit the general form of a finite volume method that ensures this property. Then we describe our method to reach such a goal. It is done in two steps. First we apply a conservative finite volume method to the homogeneous equations written in the inertial frame. Then we apply change of reference frame to the discrete equations and we derive a numerical scheme for the relative quantities.

### 2.1. General form of a conservative scheme

We consider a very general finite volume discretization of system (1)

$$h_i^{n+1} = h_i^n - \frac{\Delta t}{|C_i|}\sum_j F_{ij}^h, \tag{3}$$

$$\mathbf{q}_i^{n+1} = \mathbf{q}_i^n - \frac{\Delta t}{|C_i|}\sum_j \mathbf{F}_{ij}^q - \mathbf{C}_{1_i}^n - \mathbf{C}_{2_i}^n, \tag{4}$$

where $\mathbf{C}_1$ and $\mathbf{C}_2$ denote explicit discretizations of the Coriolis and centrifugal source terms, respectively, $h$ and $\mathbf{q} = h\mathbf{u}$ denote cell-centered values of the fluid height and momentum, respectively. The other notations are classical and we refer the reader to subsequent sections for a precise description of all the terms.

We want to ensure the conservation of the discrete inertial momentum on the whole domain (without paying attention to the *physical* loss or gain of inertial momentum due to the boundary conditions since we are interested in the *numerical* conservation property of the finite volume scheme). For a first order scheme, this would imply that the discrete relative quantities satisfy the following expression where $R$ is the rotation matrix (7) that characterizes the rotation of the domain

$$\sum_i \left(\mathbf{q}_i^{n+1} + h_i^{n+1}\boldsymbol{\Omega}\times\mathbf{x}_i\right) = R(\Delta t)\left[\sum_i (\mathbf{q}_i^n + h_i^n\boldsymbol{\Omega}\times\mathbf{x}_i)\right]. \tag{5}$$

By using (3) and (4) in (5) we can express all the quantities at time $t^n$ and obtain a relation on the whole domain between the discrete source terms, the interface fluxes and the cell-centered values. Since the finite volume method is local we can emphasize that the same relation must be satisfied on each cell, up to a conservative flux. We thus derive the only general form of the discrete first order Coriolis and centrifugal source terms that can ensure the conservation of the inertial momentum

$$\mathbf{C}_{1_i}^n + \mathbf{C}_{2_i}^n = \Delta t\frac{2}{\Omega\Delta t}\sin\left(\frac{\Omega\Delta t}{2}\right)\left[\boldsymbol{\Omega}\times\mathbf{q}_i^n + h_i^n\boldsymbol{\Omega}\times(\boldsymbol{\Omega}\times\mathbf{x}_i)\right] - \frac{\Delta t}{|C_i|}\sum_j\left[F_{ij}^h(\boldsymbol{\Omega}\times\mathbf{x}_i) + \tilde{\mathbf{F}}_{ij}\right], \tag{6}$$

where $\tilde{\mathbf{F}}_{ij}$ is any conservative momentum flux. We recognize in this formal investigation two terms which can be related to classical ones, the explicit centered discretization of the centrifugal term (second term on the right hand side) and the half of the explicit centered Coriolis term (first term on the right hand side). But the presence of a non conservative flux term (third term on the right hand side) shows that the classical fully centered discretization of the Coriolis source term cannot ensure the conservation of the inertial momentum. The remaining question is to identify the unknown conservative flux $\tilde{\mathbf{F}}_{ij}$ that appears in this third term.

### 2.2. Discretization of the equations on the rotating mesh

We first introduce some definitions related to the rotation of the domain and we exhibit the relations that exist between the inertial and relative frames. Let $\boldsymbol{\Omega}$ denote the rotation vector which is supposed to be orthogonal to the $(x,y)$ plane. We use $\Omega$ for the angular velocity of rotation of the domain. Throughout the paper we suppose that this rotation rate is constant. We introduce the related rotation matrix

$$R(t) = \begin{bmatrix}\cos(\Omega t) & \sin(\Omega t)\\ -\sin(\Omega t) & \cos(\Omega t)\end{bmatrix}. \tag{7}$$

The relative and inertial quantities (coordinates, water height, velocity) are then related by the following expressions:

$$\mathbf{x}^{\mathbf{r}} = R(t)\mathbf{x}^{\mathbf{i}}, \quad h(\mathbf{x}^{\mathbf{r}},t) = \hat{h}(\mathbf{x}^{\mathbf{i}},t), \quad \mathbf{u}(\mathbf{x}^{\mathbf{r}},t) = R(t)(\hat{\mathbf{u}}(\mathbf{x}^{\mathbf{i}},t) - \boldsymbol{\Omega}\times\mathbf{x}^{\mathbf{i}}). \tag{8}$$

Let us now introduce some definitions concerning the discretization of the domain. Let $C_i^n$ denote a cell at time $t^n$ and $\Gamma_{ij}^n$ the edge between cells $C_i^n$ and $C_j^n$. The finite volume of integration $V_i^{n+\frac{1}{2}}$ in the $(x,y,t)$ space is thus bounded by $C_i^n$, $C_i^{n+1}$ and the lateral surfaces $S_{ij}^{n+\frac{1}{2}}$ which are obtained from the evolution of $\Gamma_{ij}(t)$ during the time step $[t^n, t^{n+1}]$. Since the domain is rotating in the inertial frame, these lateral surfaces are not included in a plane. and the control volume $V_i^{n+\frac{1}{2}}$ is not a cylinder. To deal with 2D moving mesh may thus lead to complex computations and one often needs to introduce additional approximations

(see [19] for more details). But here the movement of the mesh is known a priori to be a simple rotation and it will allows us to perform all the computations analytically. Hence the desired exact conservation property can be preserved. In the following we briefly present the main formulas that are an essential tool in the description of the rotating mesh. and we refer the reader to [15] for a very clear 1D introduction about the finite volume method on moving meshes.

The lateral surfaces $S_{ij}^{n+\frac{1}{2}}$ can be described through the expression of their unit outward normal vector

$$\hat{\mathbf{n}}_{ij}(\mathbf{x}_{ij}^n, t) = \frac{1}{\sqrt{1 + \left[(\boldsymbol{\Omega} \times \mathbf{x}_{ij}^n).\tilde{\mathbf{n}}_{ij}^{xy}(t^n)\right]^2}} \begin{pmatrix} \tilde{\mathbf{n}}_{ij}^{xy}(t) \\ -(\boldsymbol{\Omega} \times \mathbf{x}_{ij}^n).\tilde{\mathbf{n}}_{ij}^{xy}(t^n) \end{pmatrix} \tag{9}$$

where the notation $\mathbf{x}_{ij}^n$ stands for a current point of $\Gamma_{ij}^n$. The vector $\tilde{\mathbf{n}}_{ij}^{xy}(t)$ denotes the unit outward normal vector (in the $(x,y)$ plane) to $\Gamma_{ij}(t)$ and thus is the space component of the outward normal vector to the lateral surface. The scalar product $(\boldsymbol{\Omega} \times \mathbf{x}_{ij}(t)).\tilde{\mathbf{n}}_{ij}^{xy}(t)$ denotes the time component of the outward normal vector to the lateral surface and does not depend on time. It thus can be considered at initial time $t^n$.

When integrations on the lateral surface $S_{ij}^{n+\frac{1}{2}}$ are considered it is natural to introduce a pair of curvilinear coordinates $(\mathbf{x}, \sigma)$ that describes this surface. For further computations we need to know how the arclength coordinate $\sigma$ can be related to time $t$. Since the mesh is simply rotating the relation reduces to the following linear function

$$t = t^n + \frac{\sigma}{\sqrt{1 + [(\boldsymbol{\Omega} \times \mathbf{x}_{ij}^n).\tilde{\mathbf{n}}_{ij}^{xy}(t^n)]^2}}. \tag{10}$$

We present a derivation of formula (9) and (10) in the Appendix A.

We can now perform the discretization of the equations on the moving mesh. We consider the system in the inertial frame (2). We integrate it on the control volume $V_i^{n+\frac{1}{2}}$ and then use the previous expressions to derive relations on the relative fluid height and momentum. Here we just present the main results of the derivation. A detailed proof for the momentum equation is given in the Appendix B.

Let us begin with the mass equation. We integrate the first equation of system (2) on the control volume. Then we apply the Green's formula and use relations (9) and (10) to obtain

$$\begin{aligned} \int_{V_i^{n+\frac{1}{2}}} \left[ \left( \frac{\partial \hat{h}}{\partial t} \right)_i + \nabla_i.(\hat{h}\hat{\mathbf{u}}) \right] dv^i = & \int_{C_i^{n+1}} \hat{h}(t^{n+1}, x^i, y^i) dx^i dy^i - \int_{C_i^n} \hat{h}(t^n, x^i, y^i) dx^i dy^i + \int_{\sum_j \Gamma_{ij}^n \times [t^n, t^{n+1}]} \hat{h}\hat{\mathbf{u}}(t, \mathbf{x}_{ij}^i(t, \mathbf{x}_{ij}^n)).\tilde{\mathbf{n}}_{ij}^{xy}(t) dt d\mathbf{x}_{ij}^n \\ & - \int_{\sum_j \Gamma_{ij}^n \times [t^n, t^{n+1}]} \hat{h}(t, \mathbf{x}_{ij}^i(t, \mathbf{x}_{ij}^n))(\boldsymbol{\Omega} \times \mathbf{x}_{ij}^i(t, \mathbf{x}_{ij}^n)).\tilde{\mathbf{n}}_{ij}^{xy}(t) dt d\mathbf{x}_{ij}^n. \end{aligned} \tag{11}$$

Since the rotating mesh is fixed in the relative frame, we can equate $\mathbf{x}_{ij}^n$ with $\mathbf{x}_{ij}^r$ and then introduce the relative fluid height and velocity using relations (8). This leads to some balancing phenomenon between the two last terms on the right hand side in (11) and we finally obtain

$$\int_{C_i} h(t^{n+1}, x, y) dx dy = \int_{C_i} h(t^n, x, y) dx dy + \int_{\sum_j \Gamma_{ij} \times [t^n, t^{n+1}]} h\mathbf{u}(t, \mathbf{x}_{ij}).\mathbf{n}_{ij} dt d\mathbf{x}_{ij}. \tag{12}$$

Thus we recover the classical finite volume discretization, on a fixed mesh, of the continuous mass Eq. (1) written in the relative frame.

We now consider the momentum equation. The main difference is that the balancing phenomenon is now incomplete and some terms involving the rotation matrix remain in the equation. They characterize the Coriolis and the centrifugal effects. We integrate the momentum equation of system (2), written in the inertial frame, on the control volume and then use same techniques as for the mass equation. The detailed computations are presented in the Appendix B. We finally obtain the following relation:

$$\begin{aligned} \int_{C_i} (h\mathbf{u})(t^{n+1}, x, y) dx dy = & R(t^{n+1} - t^n) \int_{C_i} h\mathbf{u}(t^n, x, y) dx dy - \int_{C_i} h(t^{n+1}, x, y) \boldsymbol{\Omega} \times \mathbf{x} dx dy + R(t^{n+1} - t^n) \int_{C_i} h(t^n, x, y) \boldsymbol{\Omega} \times \mathbf{x} dx dy \\ & - \int_{\sum_j \Gamma_{ij} \times [t^n, t^{n+1}]} R(t^{n+1} - t) \left[ (h\mathbf{u} \otimes \mathbf{u}) + \frac{gh^2}{2} I_2 \right] (t, \mathbf{x}_{ij}).\mathbf{n}_{ij} dt d\mathbf{x}_{ij} \\ & - \int_{\sum_j \Gamma_{ij} \times [t^n, t^{n+1}]} (h\mathbf{u}(t, \mathbf{x}_{ij}).\mathbf{n}_{ij}) R(t^{n+1} - t)(\boldsymbol{\Omega} \times \mathbf{x}_{ij}) dt d\mathbf{x}_{ij}. \end{aligned} \tag{13}$$

Note that we do not recover the classical Coriolis and centrifugal terms that come from an explicit centered discretization of continuous momentum equation written in the relative frame (1), in particular a new flux term appears on the right hand side. This is consistent with the general relation (6) that we previously derived. We notice that relation (13) is analytically exact and does not imply any discretization error.

### 2.3. The conservative scheme

Let us now introduce some classical mean value conservative quantities

$$h_i^n = \frac{1}{|C_i|}\int_{C_i} h(t^n,x,y)dxdy, \qquad \mathbf{q}_i^n = \frac{1}{|C_i|}\int_{C_i} (h\mathbf{u})(t^n,x,y)dxdy.$$

We also introduce the time step $\Delta t = t^{n+1} - t^n$ and the center $\mathbf{x}_i$ of the cell $C_i$. In the following the notation $\mathbf{x}_{ij}$ stands for the middle of the interface $\Gamma_{ij}$. For the flux terms we introduce the classical mass and momentum fluxes $F_{ij}^h$ and $\mathbf{F}_{ij}^q$ which are respectively consistent approximations of the following interface integrals computed on a fixed mesh

$$\int_{\Gamma_{ij}} h\mathbf{u}(t^*,\mathbf{x}_{ij}).\mathbf{n}_{ij}d\mathbf{x}_{ij}, \qquad \int_{\Gamma_{ij}} \left[(h\mathbf{u}\otimes\mathbf{u}) + \frac{gh^2}{2}I_2\right](t^*,\mathbf{x}_{ij}).\mathbf{n}_{ij}d\mathbf{x}_{ij},$$

where $t^*$ is defined in order to reach the accuracy we need (for example $t^* = t^n$ for first order accuracy, $t^* = t^{n+1/2}$ for second order accuracy).

Now we propose the following scheme

$$h_i^{n+1} = h_i^n - \frac{\Delta t}{|C_i|}\sum_j F_{ij}^h, \tag{14}$$

$$\begin{aligned}\mathbf{q}_i^{n+1} = \mathbf{q}_i^n &- \frac{\Delta t}{|C_i|}\tilde{R}\left(\frac{\Delta t}{2}\right)\sum_j \mathbf{F}_{ij}^q - \Delta t\tilde{R}\left(\frac{\Delta t}{2}\right)(\boldsymbol{\Omega}\times\mathbf{q}_i^n) \qquad (I)\\ &- h_i^{n+1}\boldsymbol{\Omega}\times\mathbf{x}_i + h_i^n R(\Delta t)\boldsymbol{\Omega}\times\mathbf{x}_i \qquad (II)\\ &- \frac{\Delta t}{|C_i|}\tilde{R}\left(\frac{\Delta t}{2}\right)\sum_j (F_{ij}^h\boldsymbol{\Omega}\times\mathbf{x}_{ij}), \qquad (III)\end{aligned} \tag{15}$$

where $\tilde{R}(\frac{\Delta t}{2})$ denotes the following matrix

$$\tilde{R}\left(\frac{\Delta t}{2}\right) = \frac{2}{\Omega\Delta t}\sin\left(\frac{\Omega\Delta t}{2}\right)R\left(\frac{\Delta t}{2}\right) \tag{16}$$

The conservative scheme (14) and (15) is deduced from relations (12) and (13) by using the exact integration of the rotation matrix on the time step

$$\int_{t_1}^{t_2} R(t)dt = \frac{2}{\Omega}\sin\left(\frac{\Omega(t_2-t_1)}{2}\right)R\left(\frac{t_2+t_1}{2}\right) \tag{17}$$

and the difference between rotation matrices at the beginning and at the end of the time step

$$[R(t_2) - R(t_1)]\mathbf{x} = -\frac{2}{\Omega}\sin\left(\frac{\Omega(t_2-t_1)}{2}\right)R\left(\frac{t_2+t_1}{2}\right)[\boldsymbol{\Omega}\times\mathbf{x}]. \tag{18}$$

We also notice that Term II in (15) is a second order approximation of the term

$$-\int_{C_i} h(t^{n+1},x,y)\boldsymbol{\Omega}\times\mathbf{x}dxdy + R(t^{n+1}-t^n)\int_{C_i} h(t^n,x,y)\boldsymbol{\Omega}\times\mathbf{x}dxdy,$$

that appears on the right hand side of the discrete equation for the momentum (13). It follows that the order of Scheme (14) and (15) is related to the order of the approximation of the classical fluxes $F_{ij}^h$ and $\mathbf{F}_{ij}^q$.

The main result of this subsection is that the finite volume scheme (14) and (15) is conservative for the inertial momentum. This property is characterized by relation (5) and is obvious when we consider the equivalent form of relation (15)

$$\mathbf{q}_i^{n+1} + h_i^{n+1}\boldsymbol{\Omega}\times\mathbf{x}_i - R(\Delta t)[\mathbf{q}_i^n + h_i^n\boldsymbol{\Omega}\times\mathbf{x}_i] = -\frac{\Delta t}{|C_i|}\tilde{R}\left(\frac{\Delta t}{2}\right)\sum_j \mathbf{F}_{ij}^q - \frac{\Delta t}{|C_i|}\tilde{R}\left(\frac{\Delta t}{2}\right)\sum_j (F_{ij}^h\boldsymbol{\Omega}\times\mathbf{x}_{ij}) \tag{19}$$

### 2.4. Coriolis flux and centrifugal effect

Now we are interested in a deeper analysis of the scheme (14) and (15) since we want to identify the Coriolis and centrifugal effects in momentum Eq. (15). We first observe that this equation involves in Term I two classical discrete quantities, i.e. the momentum flux and a half of the centered Coriolis term. Note that the presence of this second term is in accordance with the general characterization of a conservative scheme (6). Nevertheless Terms II and III are not easy to analyse. In particular the scheme does neither involve the full classical Coriolis and centrifugal terms nor the particular form of the Coriolis flux term that appears in (6). Hence Coriolis and centrifugal effects can not be considered separately at this stage since they are both included, at least for parts of them, in Terms II and III that appear in momentum Eq. (15).

We emphasized in (6) that a necessary condition for the conservation of the inertial momentum is that a part of the Coriolis effect has to be discretized through a non conservative flux term that involves the mass flux. Term III in (15) also involves the mass fluxes but is in conservative form. The idea is to introduce the center of the cell $\mathbf{x}_i$ in Term III

$$\sum_j (F_{ij}^h \mathbf{\Omega} \times \mathbf{x}_{ij}) = \sum_j (F_{ij}^h \mathbf{\Omega} \times (\mathbf{x}_{ij} - \mathbf{x}_i)) + \sum_j (F_{ij}^h \mathbf{\Omega} \times \mathbf{x}_i). \tag{20}$$

In the second term on the right hand side we express the mass flux $F_{ij}^h$ in term of $h_i^{n+1} - h_i^n$ by using the scheme for the fluid height (14). We finally obtain from relation (15)

$$\begin{aligned} \mathbf{q}_i^{n+1} = \mathbf{q}_i^n &- \frac{\Delta t}{|C_i|} \tilde{R}\left(\frac{\Delta t}{2}\right) \sum_j \mathbf{F}_{ij}^q \\ &- \Delta t \tilde{R}\left(\frac{\Delta t}{2}\right)(\mathbf{\Omega} \times \mathbf{q}_i^n) - \frac{\Delta t}{|C_i|} \tilde{R}\left(\frac{\Delta t}{2}\right) \sum_j (F_{ij}^h \mathbf{\Omega} \times (\mathbf{x}_{ij} - \mathbf{x}_i)) \qquad \text{(V)} \\ &+ h_i^n \left(R(\Delta t) - \tilde{R}\left(\frac{\Delta t}{2}\right)\right) \mathbf{\Omega} \times \mathbf{x}_i + h_i^{n+1} \left(\tilde{R}\left(\frac{\Delta t}{2}\right) - R(0)\right) \mathbf{\Omega} \times \mathbf{x}_i. \qquad \text{(VI)} \end{aligned} \tag{21}$$

In the following we show that Term V in (21) characterizes the Coriolis effect whereas Term VI models the centrifugal one.

Let us begin with the Coriolis part. First part of Term V is a classical centered discretization of the half of the Coriolis effect. We show in the following that the second part of Term V is also related to the Coriolis effect. For the simplicity of the analysis we restrict ourselves to a structured cartesian mesh and we assume that the mass flux can be written

$$F_{ij}^h = |\Gamma_{ij}| \mathbf{q}_{ij} . \mathbf{n}_{ij} \tag{22}$$

for some interface values $\mathbf{q}_{ij}$ of the momentum and where $\mathbf{n}_{ij}$ denotes the outside normal vector to the edge $\Gamma_{ij}$. Nevertheless we claim that the construction is valid for any mesh.

Since we consider a cartesian grid we have the relation

$$2(\mathbf{x}_{ij} - \mathbf{x}_i) = |\Gamma'_{ij}| \mathbf{n}_{ij}, \tag{23}$$

where $\Gamma'_{ij}$ is the cell edge that is orthogonal to $\Gamma_{ij}$. It follows that the second part of Term V can be written as

$$\begin{aligned} \frac{\Delta t}{|C_i|} \tilde{R}\left(\frac{\Delta t}{2}\right) \sum_j (F_{ij}^h \mathbf{\Omega} \times (\mathbf{x}_{ij} - \mathbf{x}_i)) &= \frac{\Delta t}{|C_i|} \tilde{R}\left(\frac{\Delta t}{2}\right) \sum_j \frac{\Gamma_{ij} \Gamma'_{ij}}{2} (\mathbf{q}_{ij} . \mathbf{n}_{ij}) \mathbf{\Omega} \times \mathbf{n}_{ij} = \Delta t \tilde{R}\left(\frac{\Delta t}{2}\right) \left[\mathbf{\Omega} \times \frac{1}{2} \sum_j (\mathbf{q}_{ij} . \mathbf{n}_{ij}) \mathbf{n}_{ij}\right] \\ &= \Delta t \tilde{R}\left(\frac{\Delta t}{2}\right) \left(\mathbf{\Omega} \times \left[\left(\frac{\mathbf{q}_{i1} + \mathbf{q}_{i3}}{2} . \mathbf{n}_{i1}\right) \mathbf{n}_{i1} + \left(\frac{\mathbf{q}_{i2} + \mathbf{q}_{i4}}{2} . \mathbf{n}_{i2}\right) \mathbf{n}_{i2}\right]\right), \end{aligned}$$

where, in the last equality, the indices refer to the four edges of the cell $C_i$. At first order we recognize a discrete approximation of half of the Coriolis term where the following approximation is considered for the cell momentum (written in the orthonormal basis $(\mathbf{n}_{i1}, \mathbf{n}_{i2})$)

$$\left(\frac{(\mathbf{q}_n)_{i1} + (\mathbf{q}_n)_{i3}}{2} \frac{(\mathbf{q}_n)_{i2} + (\mathbf{q}_n)_{i4}}{2}\right)^T.$$

We conclude by noting that the form of the second part of Term V is in accordance with the general relation (6) by taking

$$\tilde{\mathbf{F}}_{ij} = -F_{ij}^h \mathbf{\Omega} \times \mathbf{x}_{ij}. \tag{24}$$

Let us now consider the centrifugal effect. We use the relations (17) and (18) on the rotation matrix to write Term VI as

$$-\left[\int_0^{\Delta t} \frac{2}{\Omega \Delta t} \sin\left(\frac{\Omega t}{2}\right) \left(h_i^n R\left(\Delta t - \frac{t}{2}\right) + h_i^{n+1} R\left(\frac{t}{2}\right)\right) dt\right] (\mathbf{\Omega} \times (\mathbf{\Omega} \times \mathbf{x})).$$

At first order we recognize the semi-implicit centered discretization of the centrifugal term

$$-\Delta t \frac{h_i^n + h_i^{n+1}}{2} (\mathbf{\Omega} \times (\mathbf{\Omega} \times \mathbf{x})). \tag{25}$$

## 3. Numerical results

In this section we have two main goals. The first one is to illustrate the improvement in the conservation of discrete inertial momentum. The second is to focus on the new discretization of the Coriolis term and to study its numerical impact.

### 3.1. Conservation of the inertial momentum

We first present some numerical results that illustrate the lack of conservativity for the inertial momentum of the classical centered method.

We consider the very simple case of a stationary vortex centered at the origin. The initial profile of the velocity is given in polar coordinates

$$\mathbf{u}(\theta, r) = \begin{pmatrix} 0 \\ u_\theta(r) \end{pmatrix}, \qquad u_\theta(r) = \begin{cases} \alpha r & \text{if } r \leqslant R, \\ \alpha(2R - r) & \text{if } R \leqslant r \leqslant 2R, \\ 0 & \text{otherwise.} \end{cases} \tag{26}$$

The stationary profile of the fluid height is given by

$$gh'(r) = \frac{u_\theta^2}{r} + 2\Omega u_\theta + \Omega^2 r,$$

where $h'(r)$ denote the radial derivative of the water height. If the computational domain is centered at the origin the numerical solution remains symmetric and the inertial momentum remains zero whatever the discretization of the source term. Here we consider the box $[-0.5, 1.0] \times [-0.5, 1.0]$ and we perform the computation on four structured and regular grids with four different grid sizes, namely $30 \times 30$, $60 \times 60$, $120 \times 120$ and $240 \times 240$ points.

The computation is performed starting from the conservative scheme (14) and (15). Eq. (21) can be used instead of (15) since there is no difference between this two equations except a reorganization of the terms. We also perform computations with the classical method based on the following centered explicit scheme

$$h_i^{n+1} = h_i^n - \frac{\Delta t}{|C_i|} \sum_j F_{ij}^h, \tag{27}$$

$$\mathbf{q}_i^{n+1} = \mathbf{q}_i^n - \frac{\Delta t}{|C_i|} \sum_j \mathbf{F}_{ij}^q - 2\Delta t \boldsymbol{\Omega} \times \mathbf{q}_i^n - \Delta t h_i^n \boldsymbol{\Omega} \times (\boldsymbol{\Omega} \times \mathbf{x}_i). \tag{28}$$

To compute the mass and momentum fluxes we use a classical first order HLL solver [9,16]. We take $\Omega = \pi/3$ and $g = 7/3$. We impose $h = 1$ at the top right corner.

In Fig. 1 we present the isolines of the initial fluid height and the initial velocity vector field.

In Fig. 2 we present the evolution in time of the total inertial momentum. As it was predicted by the theory the new discretization preserves the total inertial momentum up to the machine accuracy. For the classical discretization we observe that the total inertial momentum oscillates with time. The oscillations remain bounded even for large integration time (see Fig. 2, right). The oscillations also decrease with the refinement of the mesh (see Fig. 2, left). As shown in Fig. 3, the order of convergence, in $L^\infty$ norm, of the classical method is close to one. Note that although the test case is a stationary state no superconvergence phenomenon is observed for the classical method.

### 3.2. Coriolis effect on isotropic meshes

In many meteolorogical or climate applications the centrifugal terms are not explicitly taken into account, they are included in a modified pressure gradient, and it is usual to consider equations where only the Coriolis term appears. From

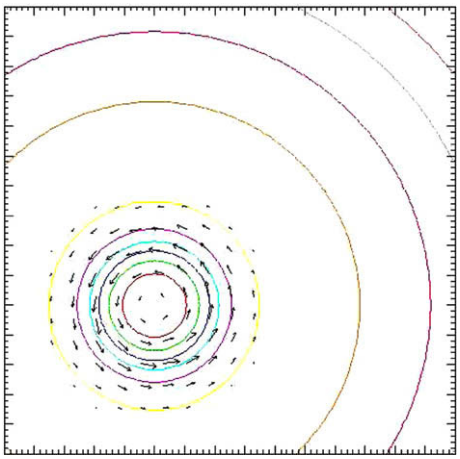

**Fig. 1.** Initial values of velocity (vector field) and fluid height (isolines) in the square $[-0.5, 1.0] \times [-0.5, 1.0]$.

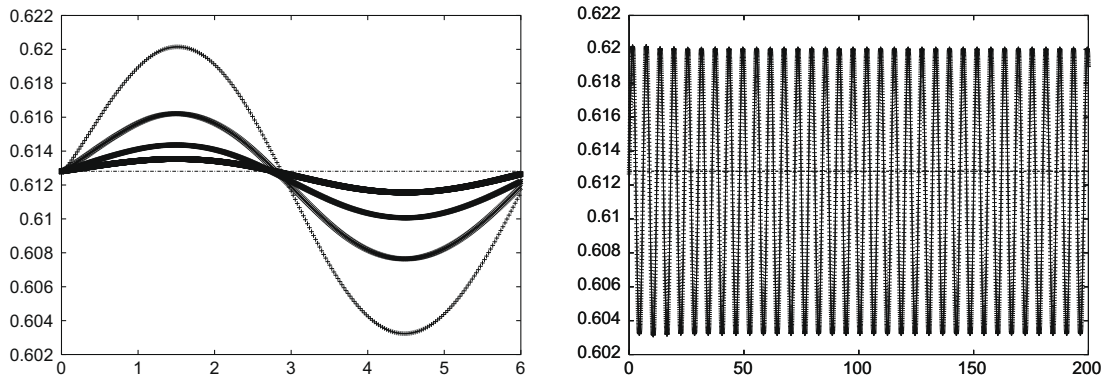


**Fig. 2.** Total inertial momentum (versus time) computed with classical method on four different meshes with 20, 40, 80 and 160 points in each direction (left) and for long time simulation (right).

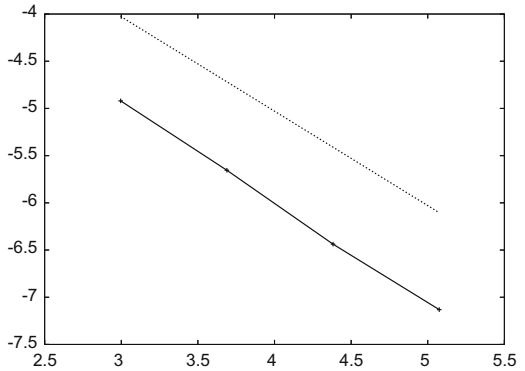


**Fig. 3.** $L^\infty$ norm of the error on the total inertial momentum (versus number of points, in Log scale) computed with the classical method on the four meshes of Fig. 2 (continuous line) compared with convergence order equal to 1. (dash line).

now on we thus neglect the centrifugal term and focus on the discretization of the Coriolis term. This is equivalent to considering shallow flow in a parabolic rotating bowl for which gravity and centrifugal effects would balance in the tangential direction. In the following we consider first order approximations of the fluxes. Hence we will also introduce first order approximations in time of the rotation matrix.

Starting from the conservative scheme (14) and (21) we derive a new first order scheme

$$h_i^{n+1} = h_i^n - \frac{\Delta t}{|C_i|}\sum_j F_{ij}^h, \tag{29}$$

$$\mathbf{q}_i^{n+1} = \mathbf{q}_i^n - \frac{\Delta t}{|C_i|}\sum_j \mathbf{F}_{ij}^q - \Delta t\boldsymbol{\Omega}\times\mathbf{q}_i^n - \frac{\Delta t}{|C_i|}\sum_j \left[F_{ij}^h\boldsymbol{\Omega}\times(\mathbf{x}_i-\mathbf{x}_{ij})\right]. \tag{30}$$

The cell-centered term on the right hand side of (30) is now identical to the classical discrete cell-centered Coriolis term that appears in (28), except for a factor of two.

In the next subsections we will compare the *centered* discretization and the *crosswind* discretization of the Coriolis effect. In particular we will study the effect of these discretizations when isotropic and nonisotropic meshes are considered and for a non-stationary Rossby adjustment problem. Since we neglect the centrifugal terms, the *centered* scheme looks like

$$h_i^{n+1} = h_i^n - \frac{\Delta t}{|C_i|}\sum_j F_{ij}^h, \tag{31}$$

$$\mathbf{q}_i^{n+1} = \mathbf{q}_i^n - \frac{\Delta t}{|C_i|}\sum_j \mathbf{F}_{ij}^q - 2\Delta t\boldsymbol{\Omega}\times\mathbf{q}_i^n, \tag{32}$$

whereas the *crosswind* scheme is written

$$h_i^{n+1} = h_i^n - \frac{\Delta t}{|C_i|}\sum_j F_{ij}^h, \tag{33}$$

$$\mathbf{q}_i^{n+1} = \mathbf{q}_i^n - \frac{\Delta t}{|C_i|}\sum_j \mathbf{F}_{ij}^q - 2\frac{\Delta t}{|C_i|}\sum_j [F_{ij}^h \mathbf{\Omega} \times (\mathbf{x}_i - \mathbf{x}_{ij})]. \tag{34}$$

In the following we will focus on these two schemes. We do not present results that are obtained with the *conservative* scheme (29) and (30). We claim that they can be seen as a meanvalue between the results obtained with centered and crosswind schemes.

We first consider the same stationary vortex as in SubSection 3.1 but we neglect the centrifugal effect. Here we consider the symmetric computational domain $[-0.5, 0.5] \times [-0.5, 0.5]$.

For the initial velocity we consider the same profile (26) as before. Since we have neglected the centrifugal effect the relation between initial velocity and fluid height is slightly different. The stationary profile of the fluid height is now given by

$$gh'(r) = \frac{u_\theta^2}{r} + 2\Omega u_\theta.$$

In Fig. 4 are presented the initial velocity (vector field) and fluid height (isolines). We take the physical value of the gravity ($g = 9.81$) and we choose $\Omega = 50$. The results are presented at time $t = 1.4$, i.e. slightly more than 11 rotations.

In Fig. 5 we present the solution with both centered and crosswind methods and for three different isotropic cartesian meshes with 20, 40 and 80 points. In Fig. 6 we also present the free surface profile along the $x$-axis. It appears that the crosswind method is more accurate than the centered one whatever the size of the mesh. In Fig. 7 we present the $L^1$ error on the numerical solution, when compared to the stationary solution, for both centered and crosswind schemes and for the three meshes. The error is of the same order of magnitude with both methods but almost two times smaller when considering the crosswind discretization of the Coriolis term. We also indicate the evolution of the $L^1$ norm of the error at final time when the mesh is refined on Fig. 8. The convergence rate is around 0.5.

### 3.3. Coriolis effect on nonisotropic meshes

Here we study the impact of the distortion of the mesh on the accuracy of the results when considering the different ways to discretize the Coriolis term.

We consider the same test case as in the previous subsection but we refine the mesh not in both directions but only in one of them (in the other one the size of the mesh remains unchanged). Here we choose to refine the mesh in the $y$-direction. More precisely we performed the computation with three different cartesian meshes for which the number of points are $20 \times 20$, $20 \times 40$, $20 \times 80$. We use periodic boundary conditions.

In Fig. 9 we show the contours of the fluid height. On the top row the crosswind discretization of the Coriolis term is used whereas on the bottom row the computation is performed with the classical centered discretization. The centered method appears to be very sensitive to the distortion of the mesh, that is, when the mesh is refined in one direction, the isolines of the fluid height tend to become parallel to the other direction. With the crosswind discretization this problem disappears and the circular symmetry of the solution is preserved quite well even if the mesh is distorted.

In Fig. 10 we also present the profile of the free surface along two axis of symmetry of the problem, the $y$-axis for the top line and the $x$-axis for the bottom line. We observe that with the crosswind discertization (C lines in the figures) the profile of the free surface is the same along the two axis and remains unchanged whatever the size of the mesh in the $y$-direction. With the centered discretization of the Coriolis term (B lines in the figures) and when the mesh is refined in the $y$-direction the profile of the free surface is more accurate in the $y$-direction but less accurate in the $x$-direction (where the fluid height tends

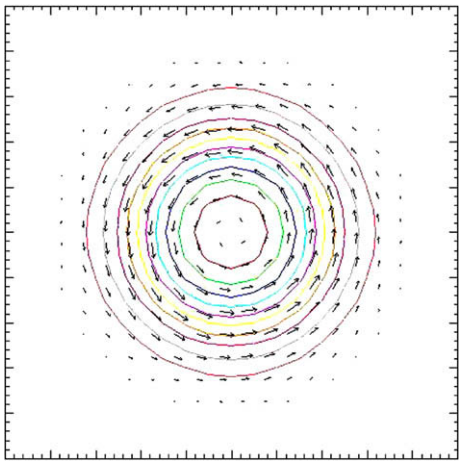

**Fig. 4.** Initial values of velocity (vector field) and fluid height (isolines) in the square $[-0.5, 0.5] \times [-0.5, 0.5]$.

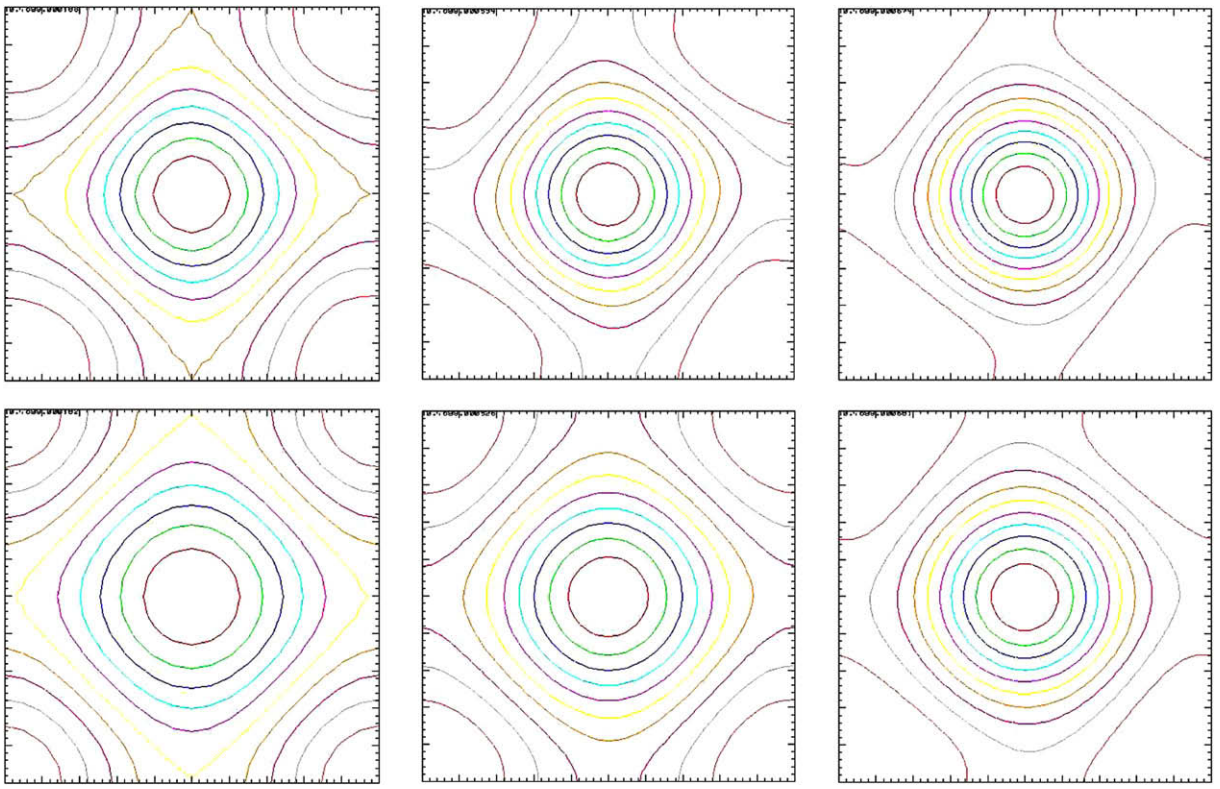

**Fig. 5.** Isolines of the computed fluid height – Crosswind (top) and centered (bottom) schemes – 20 (left), 40 (center) and 80 (right) points in both directions.

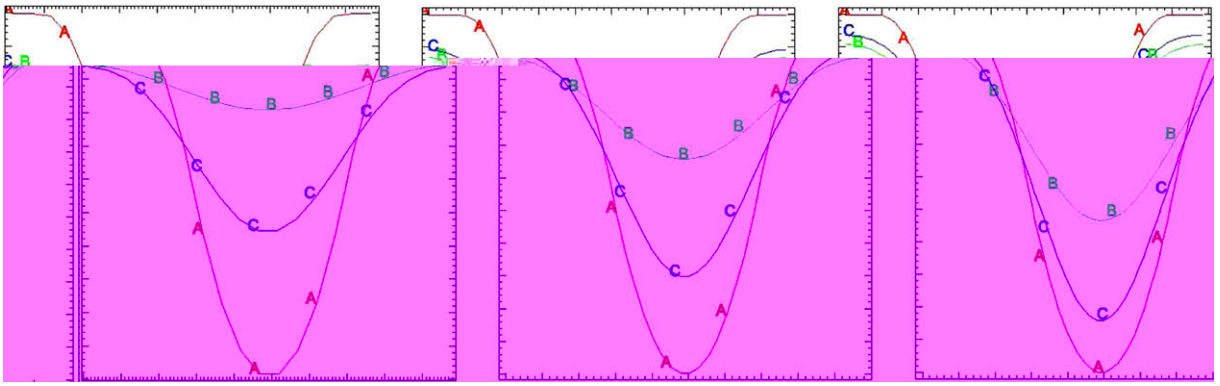

**Fig. 6.** Fluid height profiles – Cut along the horizontal axis – 20 (left), 40 (center) and 80 (right) points in both directions – Initial solution (A line), centered (B line) and crosswind (C line) schemes.

to become constant). Note also that the centered scheme is more diffusive than the crosswind one, whether the mesh is isotropic or not.

### 3.4. Rossby adjustment in an open domain

In the field of climate or meteorological simulations there is considerable interest in the study of quasi-geostrophic flows and thus the preservation of the geostrophic equilibrium. The crosswind scheme presented in this paper is not designed to preserve complex stationary states. For example the stationary vortex discussed in the previous subsection is a particular case of fully nonlinear 2D gradient wind equilibrium and is not exactly preserved by any of centered or crosswind schemes. But we notice some improvements in the crosswind scheme since the qualitative aspects of the stationary solution are preserved whether the mesh is isotropic or not as shown by the isolines of the fluid height in Fig. 9.

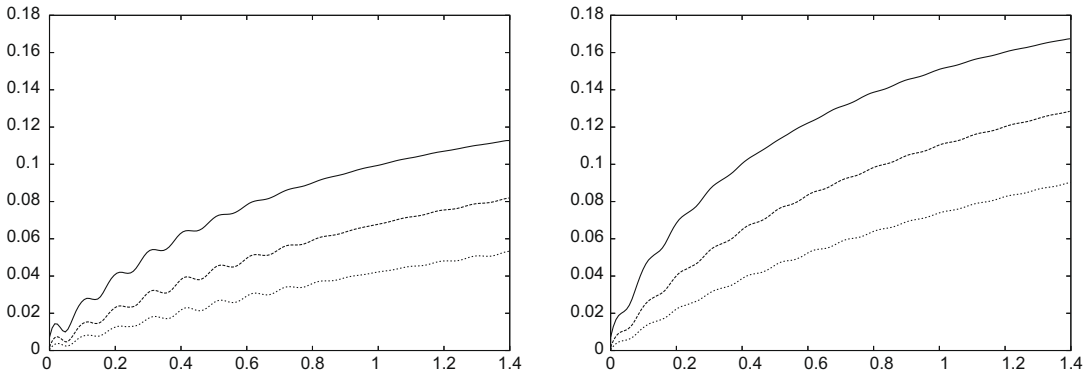


**Fig. 7.** $L^1$ norm of the error on the fluid height (versus time) – Crosswind (left) and centered (right) methods on $20 \times 20$ (continuous line), $40 \times 40$ (dash line) and $80 \times 80$ (dotted line) meshes.

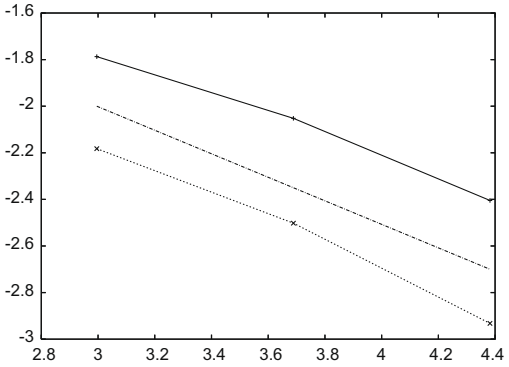


**Fig. 8.** $L^1$ norm of the error on the fluid height (versus number of points, in Log scale) computed at final time on the three meshes of Fig. 7 – Centered (continuous line) and crosswind (dotted line) methods compared with convergence order equal to 0.5 (dash line).

In this subsection we investigate a 1D problem which is related to the preservation of the geostrophic equilibrium. The study of quasi-geostrophic flows is much simpler when 1D flows are considered since the linear geostrophic equilibrium is a steady state of the fully non-linear 2D shallow water equations with 1D initial data. We thus consider in the following a particular case of the so-called Rossby adjustment, i.e. we study the relaxation of arbitrary initial configuration toward the state of linear geostrophic equilibrium. This problem was first considered by Rossby [17]. The dynamics of the adjustment is quite general, at least for small Rossby number flows. Starting from initial data with a zone which is not at equilibrium, the flow first presents a transient phase where inertial-gravity waves are emitted out of the unbalanced zone, then it adjusts in some time periods toward the geostrophic equilibrium. The geostrophic adjustment problem has received a lot of attention in numerical studies (e.g. [4,5,12]) in recent years. Here we present a 2D version of a 1D numerical test proposed in [4]. The test problem is the adjustment of a simple jet-shaped initial momentum imbalance at the initial time where a localized unidirectional velocity distribution (parallel to the $y$-axis) is superimposed to a 2D rest state. The shape of the velocity profile in $x$ is given by

$$v(x) = V\frac{(1+\tanh(4x/L+2))(1-\tanh(4x/L-2))}{(1+\tanh(2))^2}, \tag{35}$$

where $V$ and $L$ denote the maximum zonal velocity and the width of the jet. The flow is characterized by two non-dimensional parameters, namely, the Rossby $Ro$ and Burger $Bu$ numbers defined by

$$Ro = \frac{V}{fL} \qquad Bu = \frac{gH}{f^2L^2}. \tag{36}$$

The natural time scale is given by $T_f = 2\pi/f$. Here we choose $Ro = 1$, that corresponds to a fully non linear adjustment, and $Bu = 0.25$. Please note that simulations presented in this subsection have been carried out on a domain $[-150, 150] \times [-1, 1]$ and what is shown in the figures is part of this domain. In Fig. 11 we first present the fluid height and the $v$-velocity profiles in $x$-direction at time $T_f$, i.e. during the transient phase of the adjustment. As in [4] we can observe the propagation of inertial-gravity waves to the left and to the right. For the same mesh the new crosswind scheme (B line) and the centered scheme

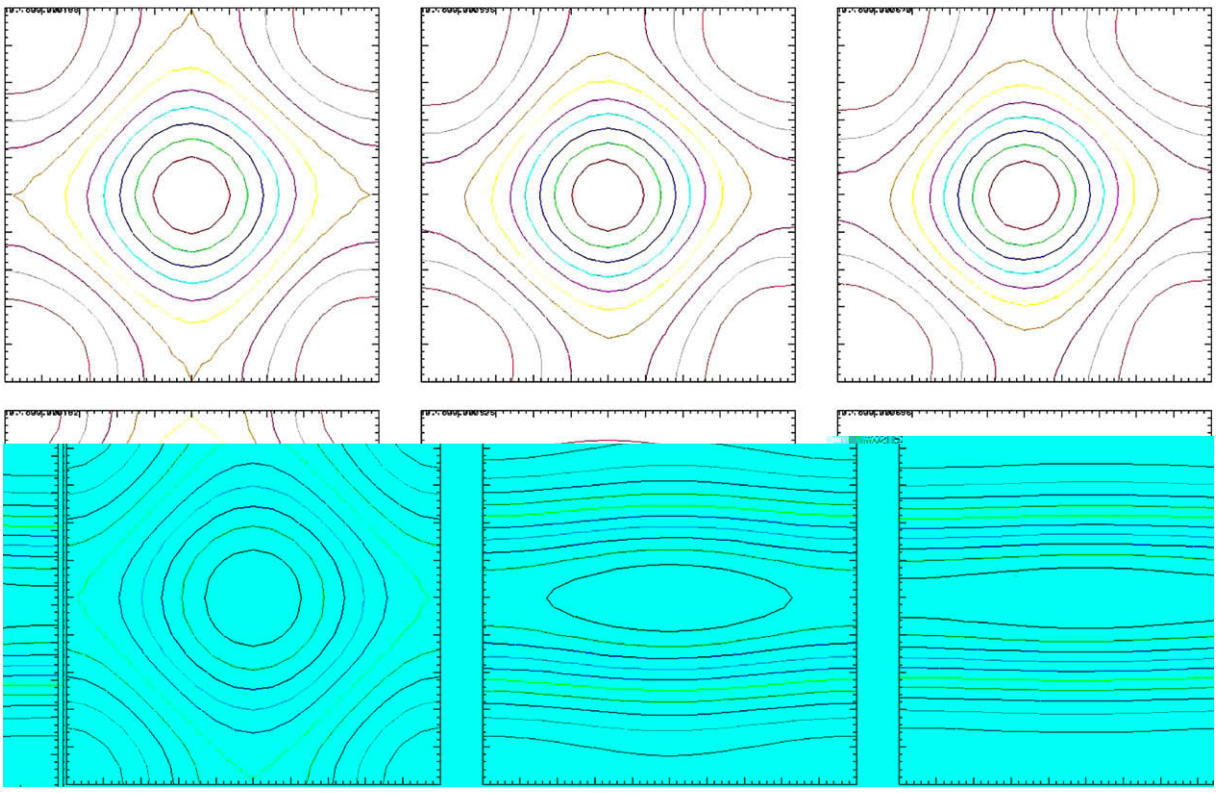

**Fig. 9.** Isolines of the computed fluid height – Crosswind (top) and centered (bottom) schemes – 20 points in the $x$-direction and 20 (left), 40 (center) and 80 (right) points in the $y$-direction.

(A line) give very similar results. Let us observe however that the crosswind scheme is a bit less diffusive. For a finer mesh we observe from the fluid height profile (C line) that the inertial-gravity waves contain two discontinuities. This result is similar to those obtain in the previous works [4,12] where the authors observed that shock formation was possible even with rotation effect, i.e. a non-zero Coriolis parameter.

Our main interest in this simulation is to focus on long time simulations in order to study the relaxation toward the equilibrium. In Fig. 12 we present the fluid height and $v$-velocity profiles at $t = 22T_f$. The qualitative aspects of the results are similar to those of [4]. We observe that the crosswind results are more accurate than the centered ones. In particular the sign of the $v$-velocity is expected to change in the adjustment zone as in [4]. This phenomenon can not be seen in the classical centered simulations with the reference mesh (A line) or even if the size of the mesh is doubled (B line).

In climate simulations there is interest in the evolution of the potential vorticity

$$\zeta = \frac{f + v_x}{h}, \tag{37}$$

which is simply advected by the flow. In Fig. 13 we present potential vorticity profiles at initial time and at $t = 22\ T_f$. We observe an important advective shift to the right during the convergence toward the geostrophic equilibrium. The results are similar to those in [4] and the difference in the profiles can be attributed to numerical diffusion in our code since we consider only first order schemes. However we observe that the crosswind scheme reduces the numerical diffusion when compared to the classical centered scheme.

## 4. Conclusion and perspectives

In this article we derive a new scheme for shallow fluid flows on rotating domains. It ensures an exact conservation of the inertial momentum. As part of this scheme we introduce a new crosswind discretization of the Coriolis term that is shown to be more accurate than the classical centered one, in particular when distorted meshes are considered. This new discretization of the Coriolis term is based on the use of the mass fluxes instead of the cell-centered momentum. The computations presented in this work are performed on cartesian meshes but we claim that the scheme can be applied on unstructured meshes. The key idea in developing the new method consists of (i) adopting a conservative discretization of the conservation laws in an inertial frame on a rotating mesh, and (ii) rewritting the resulting scheme in terms of the dependent and independent variables in the rotating frame of reference in which the grid is stationary. After some analytical manipulations

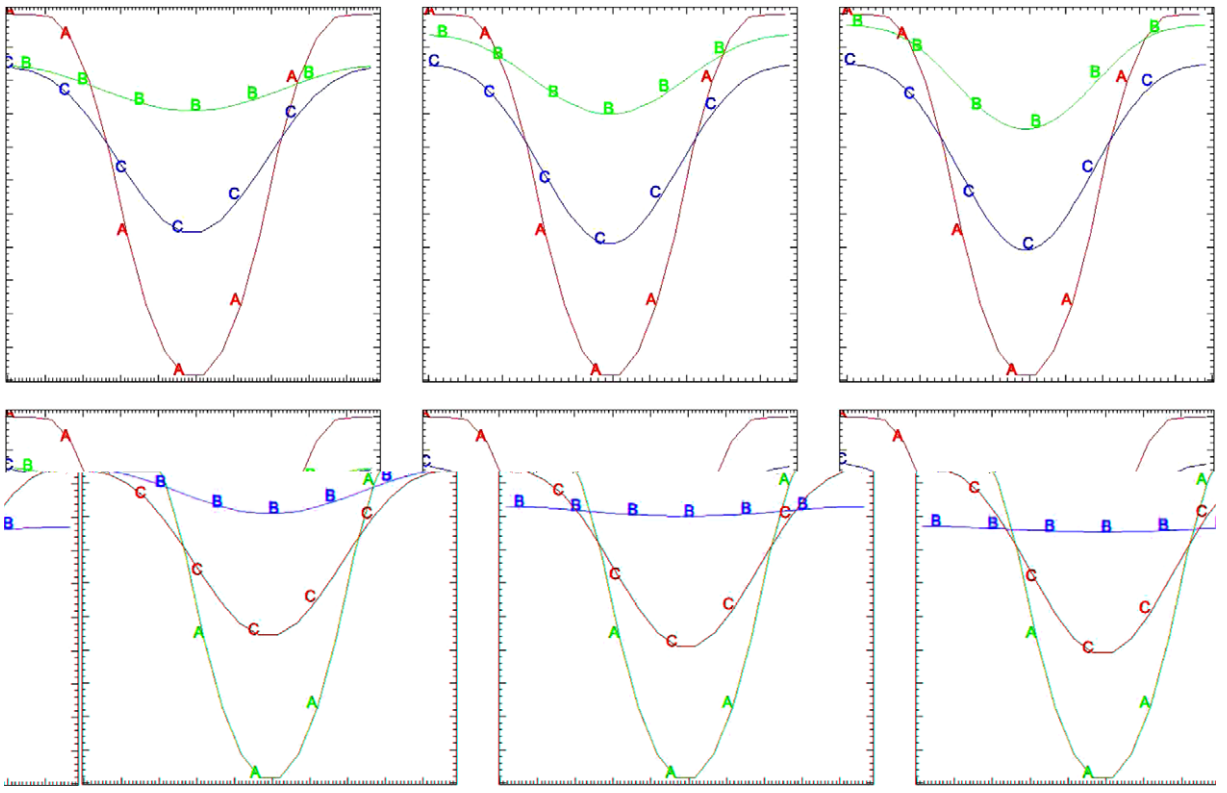

**Fig. 10.** Fluid height profiles – Cut along the vertical (top) and the horizontal (bottom) axis – 20 points in the $x$-direction and 20 (left), 40 (center) and 80 (right) points in the $y$-direction – Initial solution (A line), centered (B line) and crosswind (C line) schemes.

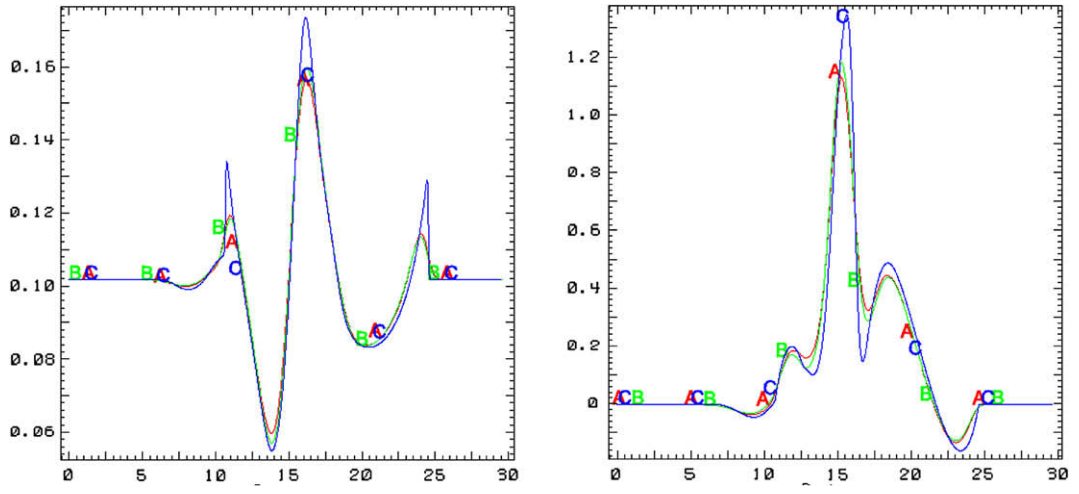


**Fig. 11.** Fluid height (left) and $v$-velocity (right) profiles (in $x$-direction) for the Rossby adjustment test case at time $t = T_f$ – Centered (A line), crosswind (B line) and reference (C line) solutions.

we identify discrete terms that correspond to the centrifugal force, and to the well-known two contributions to the Coriolis term as they appear in the classical continuum transformations of the governing equations from an inertial to a rotating frame of reference. A natural extension of this work is to consider the conservation of the angular momentum. Reviews by [7,18] show how the conservation of angular momentum plays a crucial role in the dynamics of the atmosphere, for example, in long-term oscillations phenomena such as Quasi-Biennial Oscillations, El Nino Southern Oscillations and Madden–Julian Oscillations. Climate models have failed to reproduce Quasi-Biennial Oscillations and the difficulty can be attributed to small errors in angular momentum budget [18]. This work is in progress.

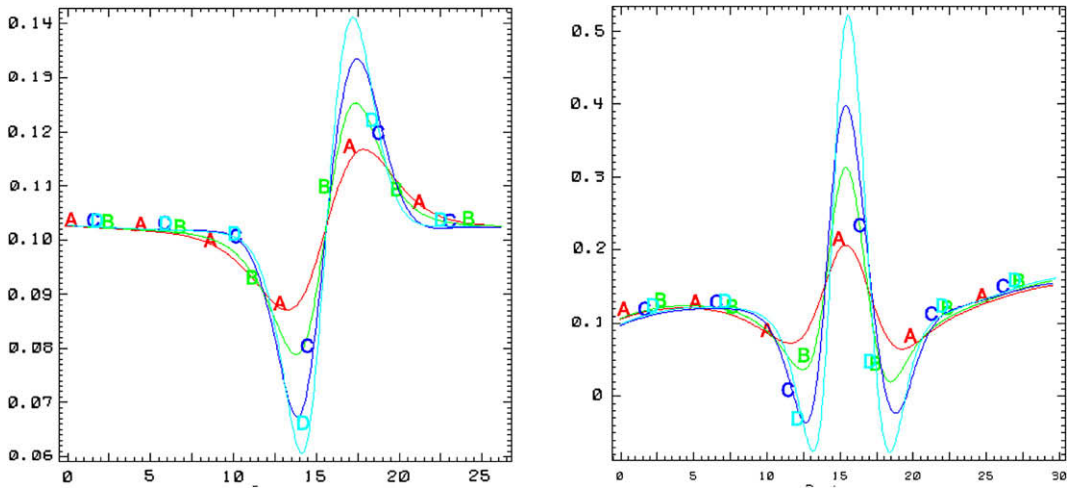

**Fig. 12.** Fluid height (left) and $v$-velocity (right) profiles (in $x$-direction) for the Rossby adjustment test case at time $t = 22.T_f$ – Centered (A & B lines) and crosswind (C & D lines) solutions on reference (A & C lines) and refined (B & D lines) meshes.

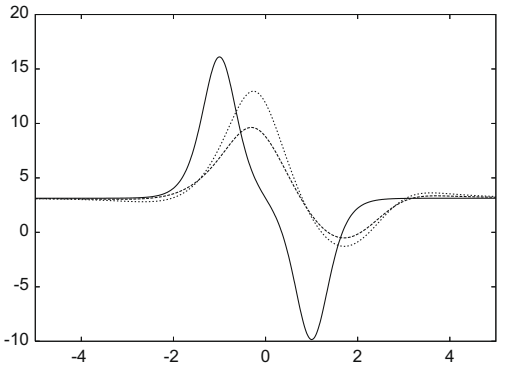

**Fig. 13.** Potential vorticity profiles (in $x$-direction) for the Rossby adjustment test case at time $t = 0$. – continuous line – and at time $t = 22T_f$ with centered – dotted line – and crosswind – small dotted line- schemes.

Clearly, in the present work we have not addressed the issue of a *well-balanced* discretization of the Coriolis force. Atmosphere–ocean flows on sufficiently large scales are almost always in nearly geostrophic balance, which means that horizontal pressure gradients are nearly in balance with the Coriolis effect. Important phenomena, such as the ubiquitous Rossby waves, are a consequence of this leading order balance. In recent years, a lot of effort has been spent on designing numerical discretizations for pdes in general [10,13], and for various geophysical flow models in particular [1–4,8,11,20], which would maintain such leading order balances automatically per construction. Such schemes provide considerable improvements of accuracy for solutions that are close to a balanced state. We are currently working on an extension of the present conservative scheme for Coriolis discretizations that combines the present ideas with the asymptotics-motivated approach to the balancing problem as in [1,2]. We hope to present this scheme elsewhere in the near future.

## Acknowledgments

The authors would like to thank M. Münch for providing the compressible numerical solver. The authors greatly acknowledge the partial support for this work from the Deutsche Forschung Gemeinschaft through grants KL 611/14 and 611/15. A sizeable part of this work was carried out at Potsdam-Institut for Climate Impact Research where R. Klein and A. Owinoh were based and they appreciate the Institute's support. The authors would also like to thank the reviewers for their useful suggestions that led to great improvement of this paper.

## Appendix A. Analysis of the rotating mesh

In this subsection we exhibit a parametrization of $S_{ij}^{n+\frac{1}{2}}$ and we compute the unit outgoing normal vector (9) at each point of the surface. We also establish the relation (10) that exists between the current time $t$ and the curvilinear coordinate $\sigma$ on the surface $S_{ij}^{n+\frac{1}{2}}$.

We perform all the computations in the inertial frame and we ignore the superscripts $i$. We denote a current point of $S_{ij}^{n+\frac{1}{2}}$ by $\mathbf{x}_{ij} = (x, y, t)$. Since $S_{ij}^{n+\frac{1}{2}}$ comes from the rotation of $\Gamma_{ij}(t)$ for $t \in [t^n, t^{n+1}]$, we can establish the following parametrization for $S_{ij}^{n+\frac{1}{2}}$

$$y_A(t)x - x_A(t)y - y_B(t)x + x_B(t)y + y_B(t)x_A(t) - x_B(t)y_A(t) = 0, \tag{38}$$

where $A(t)$ and $B(t)$ are such that $\Gamma_{ij}(t) = [A(t), B(t)]$ and

$$x_A(t) = r_A(t^n)cos(\theta_A(t^n) + \Omega(t - t^n)), \quad y_A(t) = r_A(t^n)sin(\theta_A(t^n) + \Omega(t - t^n))$$

and same thing for point $B(t)$. Note that we can also describe $S_{ij}^{n+\frac{1}{2}}$ by the following way:

$$\mathbf{x}_{ij} = (R(t - t^n)\mathbf{x}_{ij}^n, t)$$

for $t \in [t^n, t^{n+1}]$ and $\mathbf{x}_{ij}^n \in \Gamma_{ij}^n$. It implies that we can characterize a point of $S_{ij}^{n+\frac{1}{2}}$ just by giving the time $t$ and the initial coordinate $\mathbf{x}_{ij}^n$ at time $t^n$.

From (38) we can compute the outward unit normal vector to $S_{ij}^{n+\frac{1}{2}}$ at any point $\mathbf{x}_{ij}(t, \mathbf{x}_{ij}^n) = (x, y, t)$

$$\hat{\mathbf{n}}_{ij}(t, \mathbf{x}_{ij}^n) = \frac{1}{c(t, \mathbf{x}_{ij}^n)} \begin{pmatrix} y_A(t) - y_B(t) \\ x_B(t) - x_A(t) \\ \Omega(-x(x_B(t) - x_A(t)) + y(y_A(t) - y_B(t))) \end{pmatrix},$$

where $c(t, \mathbf{x}_{ij}^n)$ is such that $\|\hat{\mathbf{n}}_{ij}(t, \mathbf{x}_{ij}^n)\| = 1$. We can also write the normal vector on the compact form

$$\hat{\mathbf{n}}_{ij}(t, \mathbf{x}_{ij}^n) = \frac{1}{\sqrt{1 + [(\boldsymbol{\Omega} \times \mathbf{x}_{ij}(t, \mathbf{x}_{ij}^n)).\tilde{\mathbf{n}}_{ij}^{xy}(t)]^2}} \begin{pmatrix} \tilde{\mathbf{n}}_{ij}^{xy}(t) \\ -(\boldsymbol{\Omega} \times \mathbf{x}_{ij}(t, \mathbf{x}_{ij}^n)).\tilde{\mathbf{n}}_{ij}^{xy}(t) \end{pmatrix}, \tag{39}$$

where we exhibit the relation between the time and space components of the normal vector by introducing

$$\tilde{\mathbf{n}}_{ij}^{xy}(t) = \frac{1}{\sqrt{(y_A(t) - y_B(t))^2 + (x_B(t) - x_A(t))^2}} \begin{pmatrix} y_A(t) - y_B(t) \\ x_B(t) - x_A(t) \end{pmatrix}$$

that is the unit normal vector, in the $(x, y)$ plane, to $\Gamma_{ij}(t)$ and thus does not depend on the local coordinate $\mathbf{x}_{ij}^n$. Since $\Gamma_{ij}(t)$ is the image of $\Gamma_{ij}^n$ by the rotation $R(t - t^n)$ another way to write this vector is

$$\tilde{\mathbf{n}}_{ij}^{xy}(t) = R(t - t^n)\tilde{\mathbf{n}}_{ij}^{xy}(t^n).$$

Using this formula it follows that the product that appears in the denominator in (39) does not depend on the time since we have

$$(\boldsymbol{\Omega} \times \mathbf{x}_{ij}(t, \mathbf{x}_{ij}^n)).\tilde{\mathbf{n}}_{ij}^{xy}(t) = (\boldsymbol{\Omega} \times R(t - t^n)\mathbf{x}_{ij}^n).R(t - t^n)\tilde{\mathbf{n}}_{ij}^{xy}(t^n) = (\boldsymbol{\Omega} \times \mathbf{x}_{ij}^n).\tilde{\mathbf{n}}_{ij}^{xy}(t^n). \tag{40}$$

By using this result in (39) we obtain the relation (9). But (40) implies also that the time component on the normal vector (9) does not depend on time and thus it means that the line coming from the displacement in time of $\mathbf{x}_{ij}(t, \mathbf{x}_{ij}^n)$ is a straight line. It has for consequence the simple relation (10) between the time $t$ and a local parametrization $\sigma$ of $S_{ij}^{n+\frac{1}{2}}$.

## Appendix B. Discretization of the equations on the moving mesh

Here we present the detailed computation that we performed in Section 2.2 in order to derive a conservative discrete equation for the momentum.

We start from the integrated form of the continuous momentum equation of system (2)

$$\int_{V_i^{n+\frac{1}{2}}} \left[ \left( \frac{\partial(h\mathbf{u})}{\partial t} \right)_i + \nabla_i.(h\mathbf{u} \otimes \mathbf{u}) + \nabla_i \left( \frac{gh^2}{2} \right) \right] dv^i = 0.$$

We apply the Green's formula to obtain

$$\int_{C_i^{n+1}} \hat{h}\hat{\mathbf{u}}(t^{n+1}, x^i, y^i) dx^i dy^i - \int_{C_i^n} \hat{h}\hat{\mathbf{u}}(t^n, x^i, y^i) dx^i dy^i + \int_{S_{ij}^{n+\frac{1}{2}}} \left[ (\hat{h}\hat{\mathbf{u}} \otimes \hat{\mathbf{u}}) + \frac{g\hat{h}^2}{2} I_2 \right] (t, \mathbf{x}_{ij}^i(t, \mathbf{x}_{ij}^n)).\hat{\mathbf{n}}_{ij}^{xy}(t, \mathbf{x}_{ij}^n) d\sigma d\mathbf{x}_{ij}^n$$
$$+ \int_{S_{ij}^{n+\frac{1}{2}}} \hat{h}\hat{\mathbf{u}}(t, \mathbf{x}_{ij}^i(t, \mathbf{x}_{ij}^n)) \hat{n}_{ij}^t(\mathbf{x}_{ij}^n) d\sigma d\mathbf{x}_{ij}^n = 0.$$

We use the definition (9) of the normal vector to the surface $S_{ij}^{n+\frac{1}{2}}$ to write

$$\int_{C_i^{n+1}} \hat{h}\hat{\mathbf{u}}(t^{n+1},x^i,y^i)dx^i dy^i - \int_{C_i^n} \hat{h}\hat{\mathbf{u}}(t^n,x^i,y^i)dx^i dy^i + \int_{S_{ij}^{n+\frac{1}{2}}} \left[(\hat{h}\hat{\mathbf{u}}\otimes\hat{\mathbf{u}}) + \frac{g\hat{h}^2}{2}I_2\right](t,\mathbf{x}_{ij}^i(t,\mathbf{x}_{ij}^n)).\hat{\mathbf{n}}_{ij}^{xy}(t,\mathbf{x}_{ij}^n)d\sigma d\mathbf{x}_{ij}^n$$
$$+ \int_{S_{ij}^{n+\frac{1}{2}}} \hat{h}\hat{\mathbf{u}}(t,\mathbf{x}_{ij}^i(t,\mathbf{x}_{ij}^n))(\boldsymbol{\Omega}\times\mathbf{x}_{ij}^i(t,\mathbf{x}_{ij}^n)).\hat{\mathbf{n}}_{ij}^{xy}(t,\mathbf{x}_{ij}^n)d\sigma d\mathbf{x}_{ij}^n = 0.$$

We use the relation (10) between the time $t$ and the local coordinate $\sigma$ and the relation between the normal vector $\hat{\mathbf{n}}_{ij}^{xy}(t,\mathbf{x}_{ij}^n)$ and its unitary projection on the $(x,y)$ plane $\tilde{\mathbf{n}}_{ij}^{xy}(t)$ – see (9) – to obtain

$$\int_{C_i^{n+1}} \hat{h}\hat{\mathbf{u}}(t^{n+1},x^i,y^i)dx^i dy^i - \int_{C_i^n} \hat{h}\hat{\mathbf{u}}(t^n,x^i,y^i)dx^i dy^i + \int_{\sum_j \Gamma_{ij}^n\times[t^n,t^{n+1}]} \left[(\hat{h}\hat{\mathbf{u}}\otimes\hat{\mathbf{u}}) + \frac{g\hat{h}^2}{2}I_2\right](t,\mathbf{x}_{ij}^i(t,\mathbf{x}_{ij}^n)).\tilde{\mathbf{n}}_{ij}^{xy}(t)dtd\mathbf{x}_{ij}^n$$
$$- \int_{\sum_j \Gamma_{ij}^n\times[t^n,t^{n+1}]} \left[\hat{h}\hat{\mathbf{u}}(t,\mathbf{x}_{ij}^i(t,\mathbf{x}_{ij}^n))\otimes(\boldsymbol{\Omega}\times\mathbf{x}_{ij}^i(t,\mathbf{x}_{ij}^n))\right].\tilde{\mathbf{n}}_{ij}^{xy}(t)dtd\mathbf{x}_{ij}^n = 0. \tag{41}$$

We identify the coordinates $\mathbf{x}_{ij}^n$ and $\mathbf{x}_{ij}^r$ since the mesh is fixed in the relative frame and we introduce the relative coordinates, fluid height and velocity using relations (8) to write the third term on the left hand side as

$$\int_{\sum_j \Gamma_{ij}^n\times[t^n,t^{n+1}]} \left[(\hat{h}\hat{\mathbf{u}}\otimes\hat{\mathbf{u}}) + \frac{g\hat{h}^2}{2}I_2\right](t,\mathbf{x}_{ij}^i(t,\mathbf{x}_{ij}^n)).\tilde{\mathbf{n}}_{ij}^{xy}(t)dtd\mathbf{x}_{ij}^n$$
$$= \int_{\sum_j \Gamma_{ij}\times[t^n,t^{n+1}]} \left[(hR^{-1}(t-t^n)\mathbf{u}\otimes R^{-1}(t-t^n)\mathbf{u}) + \frac{gh^2}{2}I_2\right](t,\mathbf{x}_{ij}^r).R^{-1}(t-t^n)\mathbf{n}_{ij}dtd\mathbf{x}_{ij}^r$$
$$+ \int_{\sum_j \Gamma_{ij}\times[t^n,t^{n+1}]} [(h\boldsymbol{\Omega}\times R^{-1}(t-t^n)\mathbf{x}_{ij}^r)\otimes R^{-1}(t-t^n)\mathbf{u}(t,\mathbf{x}_{ij}^r)].R^{-1}(t-t^n)\mathbf{n}_{ij}dtd\mathbf{x}_{ij}^r$$
$$+ \int_{\sum_j \Gamma_{ij}^n\times[t^n,t^{n+1}]} [\hat{h}\hat{\mathbf{u}}(t,\mathbf{x}_{ij}^i(t,\mathbf{x}_{ij}^n))\otimes(\boldsymbol{\Omega}\times\mathbf{x}_{ij}^i(t,\mathbf{x}_{ij}^n))].\tilde{\mathbf{n}}_{ij}^{xy}(t)dtd\mathbf{x}_{ij}^n, \tag{42}$$

where we have introduced $\mathbf{n}_{ij}$, which is the normal vector to $\Gamma_{ij}$, computed in the relative frame, and which satisfies the relation

$$\tilde{\mathbf{n}}_{ij}^{xy}(t) = R^{-1}(t-t^n)\mathbf{n}_{ij}.$$

Equality (42) leads to some partial balancing phenomenon in (41). After performing the change of variables also in the two first terms of (41) we obtain ignoring the superscripts $r$

$$\int_{C_i} R^{-1}(t^{n+1}-t^n)(h\mathbf{u})(t^{n+1},x,y)dxdy - \int_{C_i} h\mathbf{u}(t^n,x,y)dxdy + \int_{C_i} h(t^{n+1},x,y)\boldsymbol{\Omega}\times R^{-1}(t^{n+1}-t^n)\mathbf{x}dxdy$$
$$- \int_{C_i} h(t^n,x,y)\boldsymbol{\Omega}\times\mathbf{x}dxdy + \int_{\sum_j \Gamma_{ij}\times[t^n,t^{n+1}]} \left[(h\mathbf{u}\otimes\mathbf{u}) + \frac{gh^2}{2}I_2\right](t,\mathbf{x}_{ij}).R^{-1}(t-t^n)\mathbf{n}_{ij}dtd\mathbf{x}_{ij}$$
$$+ \int_{\sum_j \Gamma_{ij}\times[t^n,t^{n+1}]} [(\boldsymbol{\Omega}\times\mathbf{x}_{ij})\otimes h\mathbf{u}(t,\mathbf{x}_{ij})].R^{-1}(t-t^n)\mathbf{n}_{ij}dtd\mathbf{x}_{ij} = 0. \tag{43}$$

A simple reorganization of the terms leads to the discrete momentum Eq. (13). The same computations but for the mass equation lead to a complete balancing phenomenon and then to the classical relation (12).

## References


[1] E. Audusse, F. Bouchut, M.O. Bristeau, R. Klein, B. Perthame, A fast and stable well-balanced scheme with hydrostatic reconstruction for shallow water flows, SIAM J. Sci. Comp. 29 (2004) 2050–2065.
[2] N. Botta, R. Klein, S. Langenberg, S. Lützenkirchen, Well-balanced finite volume methods for nonhydrostatic flows, JCP 196 (2004) 539–565.
[3] F. Bouchut, Nonlinear stability of finite volume methods for hyperbolic conservation laws, and well-balanced schemes for sources, Front. Math. Ser. Birkhäuser (2004).
[4] F. Bouchut, J. Le Sommer, V. Zeitlin, Frontal geostrophic adjustment and nonlinear wave phenomena in one dimensional rotating shallow water. Part 2: high-resolution numerical simulations, J. Fluid Mech. 513 (2004) 35–63.
[5] F. Bouchut, E. Scherer, V. Zeitlin, Nonlinear geostrophic adjustment of a front over an escarpment, Phys. Fluids 20 (2008) 016602.
[6] G.G. Coriolis, Mémoire sur les équations du mouvement relatif des systèmes de corps, J. l'école Polytech. 15 (1835) 142–154 (in French).

[7] J. Egger, K. Weickmann, K.P. Hoinka, Angular momentum in the global atmospheric circulation, Rev. Geophys. 45 (2007) 1–25.
[8] J.M. Greenberg, A.-Y. Leroux, A well-balanced scheme for the numerical processing of source terms in hyperbolic equations, SIAM J. Numer. Anal. 33 (1996) 1–16.
[9] A. Harten, P. Lax, B. Van Leer, On upstream differencing and Godunov type schemes for hyperbolic conservation laws, SIAM Rev. 25 (1983) 235–261.
[10] P. Jenny, B. Müller, Rankine–Hugoniot–Riemann solver considering source terms and multidimensional effects, J. Comp. Phys. 145 (1998) 575–610.
[11] B. Khouider, A. Majda, A non-oscillatory balanced scheme for an idealized tropical climate model. Part I: Algorithm and validation, Theor. Comput. Fluid Dyn. 19 (2005) 331–354.
[12] A. Kuo, L. Polvani, Time-dependent fully nonlinear geostrophic adjustment, J. Phys. Oceanogr. 27 (1997) 1614–1634.
[13] R.J. LeVeque, Balancing source terms and flux gradients in high-resolution Godunov methods: the quasi-steady wave-propagation algorithm, J. Comput. Phys. 146 (1998) 346–365.
[14] A. Majda, Introduction to PDE's and Waves for the Atmosphere and Ocean, Courant Lectures Note, vol. 9, American Mathamatical Society & Courant Institute of Mathematical Sciences, 2002.
[15] M. Meriaux, S. Piperno, Finite volume methods on moving grid for one-dimensional scalar hyperbolic equations, INRIA Report No. 4042, 2000, pp. 1–40, <http://www.inria.fr/rrrt/rr-4042.html>.
[16] M. Münch, MOLOCH, Ein Strömungsverfahren für inkompressible Strömungen, PIK Report, No. 109, <http://www.pik-potsdam.de/research/publications/pikreports>, 2008, pp. 1–88 (in German).
[17] C. Rossby, On the mutual adjustment of pressure and velocity distributions in certain simple current systems II, J. Mar. Res. 1 (1938) 239–263.
[18] J. Thuburn, Some conservation issues for the dynamical cores of NWP and climate models, JCP 227 (2008) 3715–3730.
[19] P.A. Zegeling, Moving grid methods for time-dependent PDEs, CWI Tract, 1991.
[20] V. Zeitlin, F. Bouchut, S. Medvedev, G. Reznik, A. Stegner, Nonlinear Dynamics of Rotating Shallow Water: Methods and Advances, Edited Series on Advances in Nonlinear Science and Complexity, vol. 2, Elsevier, 2007.